Selective population of states in fission fragments from the $^{32}S+^{24}Mg$ reaction

S. J. Sanders, A. Hasan, and F. W. Prosser
The University of Kansas, Department of Physics and Astronomy, Lawrence, Kansas 66045

B. B. Back, R. R. Betts, M. P. Carpenter, D. J. Henderson, R. V. F. Janssens, T. L. Khoo, E. F. Moore,* P. R. Wilt, F. L. H. Wolfs,† and A. H. Wuosmaa
Argonne National Laboratory, Argonne, Illinois 60439

K. B. Beard ‡
University of Notre Dame, Department of Physics, Notre Dame, Indiana 46556

Ph. Benet §
Purdue University, Lafayette, Indiana 47907
(Received 8 October 1993)

The symmetric and near-symmetric mass fission yields from the $^{32}S+^{24}Mg$ reaction have been studied in a particle-particle-γ coincidence measurement. Evidence is presented for a selective population of states in ^{28}Si fragments arising from the symmetric fission of the ^{56}Ni compound nucleus. A statistical-model calculation of the expected strength to specific mutual excitations of the fission fragments is presented and compared to the experimental results. This calculation is found to describe the structures observed at high excitation energy in the fission Q-value spectra quite well. Analysis of the γ-ray spectra indicates, however, that a specific set of states in ^{28}Si, corresponding to a highly deformed prolate band, is populated more strongly than expected based on a purely spin-weighted, statistical decay of the compound nucleus. It is suggested that the population pattern of states in the fission fragments may reflect nuclear structure effects at the point of scission.

PACS number(s): 25.70.Jj, 25.70.Gh, 24.60.Dr

I. INTRODUCTION

The fission-like decay of light compound nuclei ($A_{CN} < 60$) formed through heavy-ion reactions at center-of-mass energies near and above the Coulomb barrier has been the focus of a number of experimental [1–16] and theoretical studies [17–19]. One of the principal questions concerning these yields has been whether there are two (or more) distinct processes involved in their production. In all of the systems studied, there is a fully energy-damped, binary-decay component that can be understood in terms of the statistical fission of the compound nucleus. However, in some systems there appears to be an additional component in the binary yields. This component, which is generally at more positive Q values than expected for fission, is not easily encompassed in the fission picture. Two alternative mechanisms have been suggested. The first is that these yields result from a dinucleus orbiting process [1,17]. A second possibility is that they arise from trapping of the composite system within a shell-stabilized, secondary minimum of the nuclear potential-energy surface. The latter was first suggested [20] in connection with the strong resonance behavior found in the energy dependence of the large-angle elastic and inelastic scattering yields of some of these systems [20–22]. There is considerable uncertainty as to how the fission, orbiting, and resonance processes are related. To help disentangle the fission reaction components from those resulting from the other processes, there is a need to develop a more complete understanding of the fission process. In particular, the details of how the fission yield is distributed among different decay channels, including the distribution of energy and spin in the fission fragments, needs to be established. The role of nuclear structure on the decay process also needs to be delineated.

Several measurements have recently been performed to gain a better understanding of the fission process in light systems and to explore the relationships among the different reaction mechanisms. In this paper we focus on a particle-γ coincidence measurement of the $^{32}S+^{24}Mg$ reaction. The average energies and cross sections for the binary yields of this reaction have been previously found to be well described by the transition-state model for fission [8,9]. A comparison of the heavy-ion resonance behavior for the $^{32}S+^{24}Mg$ and $^{28}Si+^{28}Si$ elastic and inelastic scattering yields indicates an elastic resonance strength in the former system that is only about 4% of that observed in the latter [23], consistent with the damped, binary de-

*Present address: Dept. of Physics, North Carolina State University, Raleigh, NC 27696.
†Present address: Nuclear Structure Research Laboratory, University of Rochester, Rochester, NY 14627.
‡Present address: College of William and Mary, Williamsburg, VA 23185.
§Present address: 11 rue de Bondues, F-59200 Tourcoing, France.

cay of the $^{32}S+^{24}Mg$ system arising largely through the fission mechanism. In this context we use fission to refer to the decay of the compact, equilibrated compound nucleus into two heavy fragments. We view this as a process distinct from the binary decay of a compound system trapped in a more deformed configuration, as suggested by various orbiting and resonance models. The present work involves a study of how the fission yield is distributed among the possible mutual excitations of the fragments in the symmetric and near-symmetric mass channels. In particular, the influence of nuclear structure at the scission point on the population of states in the fragments is explored. In a companion paper we will describe a measurement of the $^{24}Mg+^{24}Mg$ reaction where there is an additional component to the binary yields that cannot be easily understood in the context of a fission process [24]. That paper will emphasize the coexistence of fission and a separate reaction mechanism corresponding to heavy-ion resonance behavior.

We note that the fission of light nuclei is restricted to a relatively narrow range of partial waves near the critical angular momentum for fusion. High barriers prevent significant fission competition for lower spin values. Since most of the rotational energy at scission is expected to contribute to the relative energy of the fragments, with a lesser amount leading to their excitation, it is possible for both fragments to be formed at energies where their respective level structures are known. These fragments may then carry information about the structure of the nuclear composite at the point of scission.

We have measured the excitation-energy spectra for the $^{24}Mg+^{32}S$ and $^{28}Si+^{28}Si$ channels from the $^{32}S+^{24}Mg$ reaction at $E_{c.m.} = 51.0$ and 54.5 MeV. The difference in these two energies was chosen to be somewhat larger than the typical width of the gross structure observed in excitation functions for the $^{28}Si+^{28}Si$ and $^{32}S+^{24}Mg$ systems. The associated γ-ray yields were also measured at the lower energy. This low energy leads to relatively little secondary light-particle emission from the ^{28}Si fragments in the mass-symmetric fission channels. The ^{28}Si fragments are particle bound up to 10 MeV and, on average, are emitted with an excitation energy of 6.5 MeV. The population of specific states in the fragments, which is stronger than expected on the basis of the statistical decay of the compound nucleus, would indicate that nuclear structure at the scission configuration has an influence on the fission process. A calculation of the expected excitation-energy and related γ-ray spectra based on the transition-state model of fission is presented and compared with the experimental results. Although the calculation is found to reproduce the main features of the data, including the observation of structure in the excitation-energy spectra of strongly damped yields, comparisons of the calculated and measured γ-ray yields suggest that the intrinsic structure of the fragments has an influence on which states are populated following fission.

The paper is organized as follows. In the next section, the details of the experimental arrangement and separate discussions of the particle-particle and particle-particle-γ coincidence measurements are presented. A calculation of the excitation-energy spectra, which is based on the transition-state model for fission, is presented in Sec. III. The results of this calculation are used in Sec. IV to highlight both those features of the data that can be readily understood within a statistical fission model (for instance, the excitation-energy spectra), as well as the observations that suggest the importance of specific nuclear configurations (from the analysis of the γ-ray spectra). A summary of the results is presented in Sec. V.

II. EXPERIMENTAL RESULTS

The experiment was performed using the Argonne-Notre Dame BGO γ-ray facility at Argonne National Laboratory [25]. Beams of 120.9 MeV and 129.0 MeV ^{32}S particles from the ATLAS accelerator were incident on a self-supporting, isotopically enriched ^{24}Mg target of 300 $\mu g/cm^2$ areal density. The corresponding beam energies at the center of the target are 119.1 and 127.2 MeV, with $^{32}S+^{24}Mg$ center-of-mass energies at the target center of 51.0 and 54.5 MeV, respectively. Additional self-supporting targets of Au (60 $\mu g/cm^2$) and carbon (100 $\mu g/cm^2$) were used for calibration, background determination, and normalization purposes.

A schematic drawing of the experimental arrangement is shown in Fig. 1. For the present measurements, the forward-angle Compton-suppressed Ge spectrometers (CSG) and some of the BGO array elements of the γ-ray facility were replaced by a particle scattering chamber in which two 20 cm $\times$ 20 cm position-sensitive, multigridded avalanche counters (MGAC's) [26] were mounted for the coincident detection of binary reaction fragments. These detectors were centered at $\pm 35°$ with respect to the beam axis and each was located $\approx$51 cm from the target. To establish the normalization of the product of beam current and target thickness, two Si (surface-

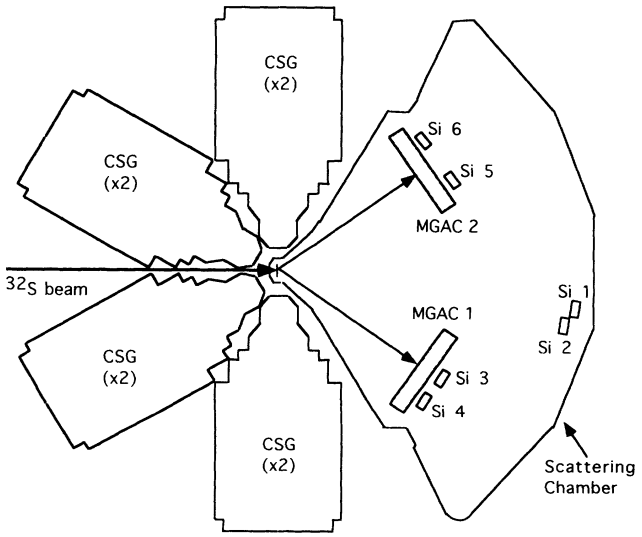

FIG. 1. Schematic drawing of the experimental arrangement. Note that the BGO array of the Argonne-Notre Dame γ-ray facility is not shown for clarity.

barrier) detectors were positioned at 8.1° and 88 cm and 10.2° and 87 cm where strong elastic yields could be compared to cross sections obtained from optical-model calculations. Four additional Si (surface-barrier) detectors were located behind the gas counters and were used to help calibrate these counters and establish their threshold behavior for detecting less ionizing particles.

Excitation-energy spectra were obtained for the symmetric and near-symmetric fission channels at both beam energies. For the measurement at $E_{\mathrm{c.m.}}$=51.0 MeV, more detailed information about the decay process was obtained through the detection of γ rays in coincidence with the fission fragments, using the CSG spectrometers of the Argonne-Notre Dame array. Eight CSG spectrometers were used, mounted above and below the reaction plane at approximately ±90° and ±145° to the beam axis. Because of the large number of transitions leading to high energy γ rays in the fragments being studied, the gain of the Ge detectors was set to allow detection of γ rays up to 10 MeV. Energy and relative efficiency calibrations of the CSG spectrometers were obtained using ^{243}Am, ^{56}Co, ^{152}Eu, and ^{182}Ta sources at the target position. The strength of the ^{56}Co source was known, allowing for an absolute efficiency calibration. The highest calibration energy, using a PuC source [27] of known strength, was 6.1 MeV. Above this energy the efficiency was extrapolated, based on the smooth exponential behavior of the calibration at lower energies.

A compact 39-element BGO array (not shown in Fig. 1) surrounded the target for angles $\theta_{\mathrm{lab}} > 65°$. Although only restricted information was obtained from this sum-energy/multiplicity array (because of the limited energy resolution of the array elements and the low multiplicity of many of the decay chains in the light systems studied), the high efficiency of the array for detecting high-energy γ rays proved useful in resolving some of the ambiguities resulting from unresolved γ-ray transitions in the Ge data.

A. Particle-particle coincidence measurements

Identification of binary reaction products was achieved by measuring the scattering angles and the difference in arrival times of the particles at the MGAC's. A mass resolution of about one mass unit (FWHM) was obtained, as shown in Fig. 2 for the coincidence data at $E_{\mathrm{c.m.}}$=51.0 MeV. The greater strength observed in the $4n$ channels with A_{fragment} = 16, 20, 24, 28, and 32 has been observed in earlier measurements and can be attributed to preferential fission decay to channels comprised of the strongly bound "α-particle-like" nuclei ^{16}O, ^{20}Ne, ^{24}Mg, ^{28}Si, and ^{32}S [9,28]. In these earlier measurements, it was also established that the fission of the ^{56}Ni compound nucleus favors more mass-asymmetric channels. The greater strength observed in this measurement for the symmetric and near-symmetric 28+28 and 24+32 channels can be attributed to a rapid falloff of the coincidence detection efficiency for the more asymmetric mass channels. The lack of symmetry about mass 28 results from the decrease in efficiency of one of the MGAC's for detecting lower mass (and, correspondingly, lower ionization) fragments. This ionization threshold behavior was not found to be a significant factor for the ^{24}Mg+^{32}S and ^{28}Si+^{28}Si channels.

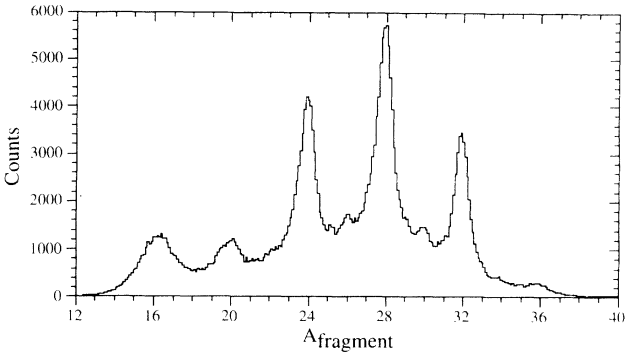

FIG. 2. Mass distribution based on the coincident detection of binary fragments in the multi-gridded avalanche counters. The data shown were obtained for $E_{\mathrm{c.m.}}$=51.0 MeV.

A coplanarity condition was imposed on the data to discriminate against events with secondary light-particle emission from the reaction fragments. The product $\hat{k} \cdot (\vec{v}_1 \times \vec{v}_2)$ was generated from the fragment velocities $\vec{v}_1$ and $\vec{v}_2$, where $\hat{k}$ is directed along the beam axis. This product should vanish for binary events that are coplanar with the beam direction, although multiple scattering in the target and the finite detector position resolution weakens the selectivity. Based on a Monte Carlo simulation of the experimental response, to be discussed further below, it is expected that about 80% of events involving secondary light-particle emission are suppressed by this condition.

Reaction Q-value spectra were obtained for the different binary-reaction channels based on the known entrance-channel parameters, the deduced mass of the fragments (as determined from Fig. 2), and the observed fragment angles. Assuming the dominance of $N = Z$ fragments in the $4n$ channels, as supported by the coincident γ-ray yields, the Q-value spectra can be converted to excitation-energy spectra, as shown in Figs. 3 and 4 for the ^{24}Mg+^{32}S and ^{28}Si+^{28}Si channels, respectively. Data at both $E_{\mathrm{c.m.}}$=51.0 and 54.5 MeV are shown to facilitate comparisons of the spectra at the two energies. Pronounced structures, common for both energies, are observed in these spectra at high excitation energies. Since the number of possible mutual excitations becomes very large above 10 MeV in these channels, the observation of high-energy structures might suggest the importance of fission fragments of specific nuclear structure. It will be shown, however, that the observed peaks are actually consistent with a spin-weighted population of the states in the final fragments.

The detection efficiency for the different mass channels at the two bombarding energies was determined by a Monte Carlo simulation of the coincidence arrangement. This simulation was also used to determine the various contributions to the experimental mass and Q-value resolutions. A $1/\sin\theta_{\mathrm{c.m.}}$ angular dependence was assumed

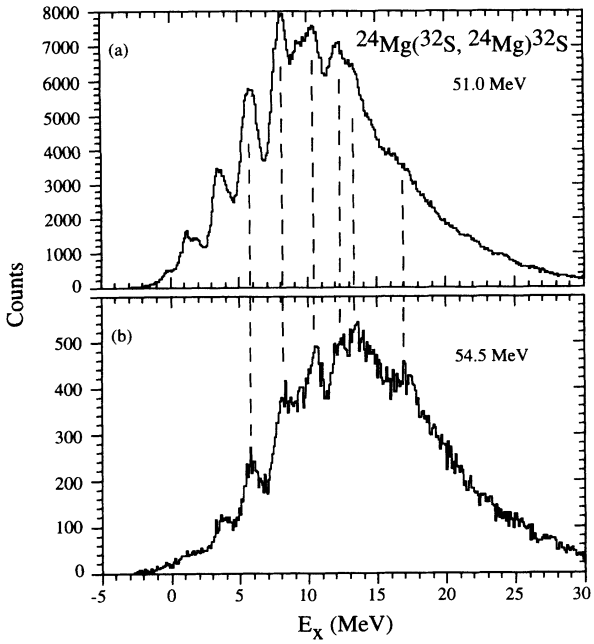

FIG. 3. Excitation-energy spectra for the ^{24}Mg(^{32}S, ^{24}Mg)^{32}S reaction at (a) $E_{c.m.}$=51.0 and (b) $E_{c.m.}$=54.5 MeV. The dashed lines are to aid in comparing the peak structure at the two energies.

for the primary fission fragments, in agreement with an earlier study of this reaction [9]. Included in the simulation were effects resulting from multiple scattering in the target, the position and time resolutions of the MGAC's, the finite beam-spot size, and the recoil effects from γ emission from the fragments. The Monte Carlo simulation was used to generate a file of pseudo-events that could be replayed using the same data analysis programs and incorporating the same criteria for event selection as used for the replay of the experimental data. These calculations, which were in good agreement with the observed mass and excitation-energy resolution, indicate that the dominant contribution to both the mass and Q-value widths is the angular spread resulting from multiple scattering in the target. To determine the effect of secondary light-particle emission on the coplanarity and mass distributions, a separate calculation was performed where it was assumed that a 9 MeV α particle was emitted isotropically from one of the fission fragments.

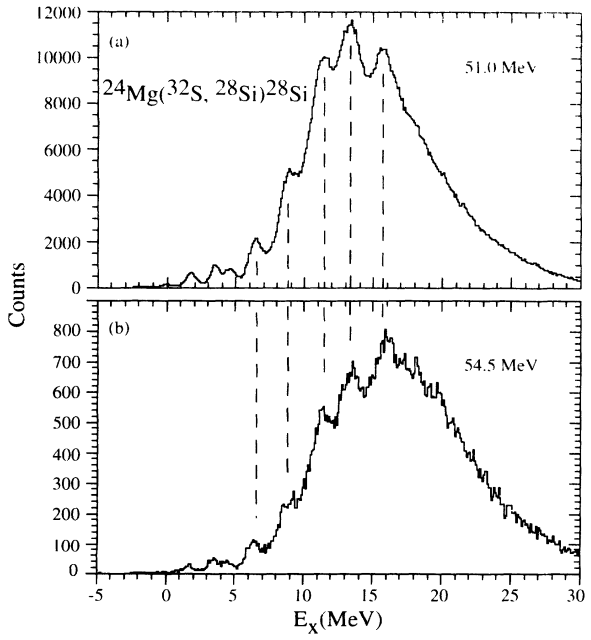

FIG. 4. Excitation-energy spectra for the ^{24}Mg(^{32}S, ^{28}Si)^{28}Si reaction at (a) $E_{c.m.}$=51.0 and (b) $E_{c.m.}$=54.5 MeV. The dashed lines are to aid in comparing the peak structure at the two energies.

B. Particle-particle-γ coincidence measurement

Doppler-shift corrections were applied to the γ-ray data on an event-by-event basis using the measured velocities of the detected fragments. Since it is not possible to know *a priori* which of the two fragments emits a given γ ray, both Doppler corrections were applied to the measured γ-ray energies. For mass-asymmetric channels, each γ ray was therefore sorted into two spectra corresponding to the masses of the two outgoing fragments. For the symmetric channel (^{28}Si+^{28}Si), each γ ray was added to the ^{28}Si-gated spectrum twice, using the two possible Doppler corrections. Since the Doppler-shift corrections are large, the γ rays from a given transition will tend to be spread out over a large range of energies when the "wrong" correction is applied, thus adding to the overall spectrum background, but without significantly adding to the photopeak structure in the spectrum. For example, when the "wrong" correction is applied to the ^{28}Si (1779 keV$\rightarrow$g.s.) transition, the counts are spread over 300 keV in the resulting spectrum. Although the counts are not spread uniformly over this range because of the limited angular coverage of the particle counters, the resulting structure is still much broader than the 1779 keV photopeak found using the proper Doppler correction. γ rays falling in one of the strongest peaks, corresponding to low-lying transitions (and including the 1779 keV photopeak), were taken as being "known," and the complementary Doppler solution was therefore suppressed.

Whereas Doppler shifts could be deduced using the particle angle and energy information, the Doppler broadening of the γ-ray lines resulting from the finite detector solid angles was still a significant problem. The γ-ray peak width in the ^{28}Si-gated spectrum, for example, changed from 13 keV at 1779 keV to 46 keV at 5110 keV. Because of this energy dependence of the width, it was found useful to display the γ-ray spectra with a logarithmic energy scale. As long as the width of the peak is proportional to the γ-ray energy, as is the case when the Doppler broadening effect dominates the resolution, this scaling leads to constant width peaks over the full range of energies. A logarithmic energy scaling is used for all of the γ-ray spectra shown in this paper. Figure 5 presents the spectra corresponding to the mass groups

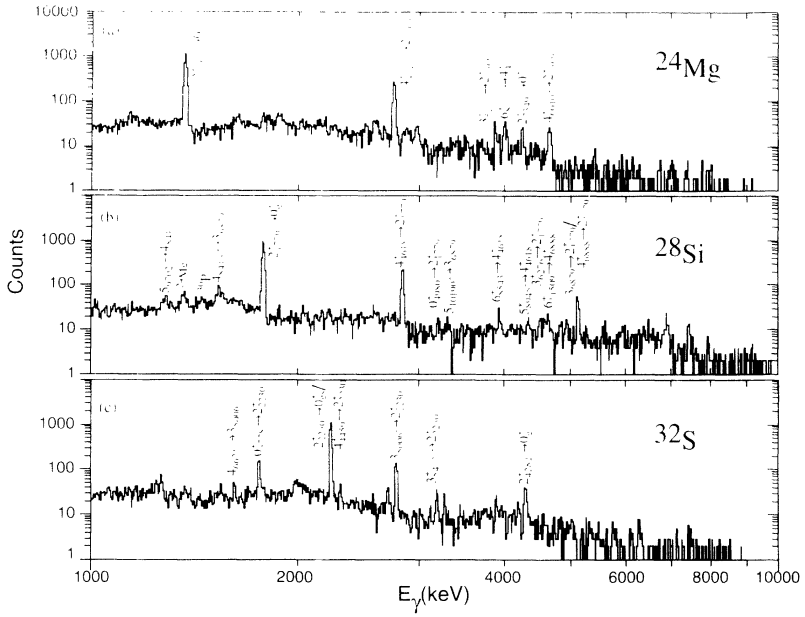

FIG. 5. γ-ray spectra in coincidence with the ^{24}Mg+^{32}S fission channel (a) and (c) and the ^{28}Si+^{28}Si channel (b) for the ^{32}S+^{24}Mg reaction at $E_{\mathrm{c.m.}}$=51.0 MeV. Doppler-shift corrections have been applied to the data according to the indicated masses (see detailed discussion in the text). A logarithmic energy scale is used to maintain constant shapes for the strongly Doppler-broadened peaks.

A_{fragment}=24, 28, and 32. Some of the stronger transitions are labeled, with levels denoted by their spin, parity, and excitation energy in keV. As expected, the $Z = A/2$ channels are found to dominate the fission process in the near-symmetric $4n$ channels.

III. TRANSITION-STATE MODEL CALCULATION OF ENERGY SPECTRA

One of the unexpected results of this measurement was the observation of relatively narrow structures ($\Gamma_{\mathrm{FWHM}} \approx 2$ MeV) in the excitation energy spectra above 10 MeV, as seen in Figs. 3 and 4. Similar structures have been noted in earlier measurements of the inelastic yields for the ^{28}Si+^{28}Si [28,30] and ^{24}Mg+^{24}Mg [31] reactions, but in both of those systems there is also a strong resonance component, and one might *a priori* be tempted to attribute these structures to a mechanism other than compound-nucleus fission. At an excitation energy of 15 MeV in the ^{28}Si+^{28}Si channels, for example, the density of possible mutual excitations of γ-decaying states reaches a level of $\approx$ 45/MeV. It might then be expected that averaging over such a large number of excitations would lead to relatively smooth energy spectra, contrary to what is observed.

To understand better the observed excitation-energy spectra, we extended the transition-state model calculations for this system [9] and calculated the expected spectra, assuming a purely spin-weighted decay of the compound nucleus. The basis for these calculations can be discussed in terms of the reaction energy balance, as indicated schematically in Fig. 6. Starting with an entrance-channel center-of-mass energy $E_{\mathrm{c.m.}}$ and orbital angular momentum ℓ_{in}, two interacting heavy ions surmount the entrance-channel barrier to form a compound nucleus of definite spin J_{CN} ($=\ell_{\mathrm{in}}$ for spinless particles in the entrance channel) and excitation energy E^*_{CN}. The effective excitation energy of the compound nucleus E^*_{eff} is determined by locating the zero point of the effective energy Δ_{eff}, with $E^*_{\mathrm{eff}} = E^*_{\mathrm{CN}} - \Delta_{\mathrm{eff}}$. This zero-point energy can be determined by assuming that the virtual ground state for the level densities should correspond to the macroscopic-energy ground state [32]. For the compound nucleus to fission, it must overcome the spin-dependent fission barrier at the saddle point. The magnitude of this barrier can be expressed in terms of the macroscopic energy of the system at the saddle point V_{saddle} and the microscopic shell corrections in this configuration $\Delta V_{\mathrm{shell}}$. The fission branching ratio $\Gamma(Z_L, A_L)$ to a channel where the lighter fragment is of nuclear charge Z_L and mass A_L, respectively, is then determined by the available phase space above the saddle point, with

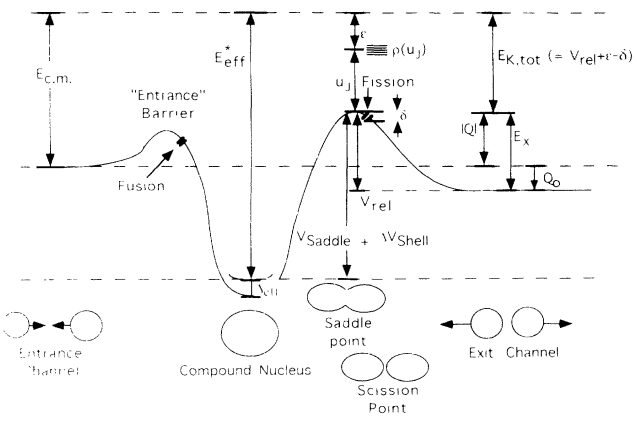

FIG. 6. Schematic illustration of the energy balance in a fusion-fission reaction.

$$\Gamma_f(Z_L, A_L) = \int_{\varepsilon=0}^{\varepsilon_{\max}} \frac{\rho_f(E^*_{\rm CN} - \Delta_{\rm eff} - V_{\rm saddle}(J_{\rm CN}, \eta) - \Delta V_{\rm shell}(J_{\rm CN}, Z_L, A_L) - \varepsilon, J_{\rm CN})}{2\pi\hbar\rho_{\rm CN}(E^*_{\rm CN} - \Delta_{\rm eff}, J_{\rm CN})} d\varepsilon \quad (1)$$

where

$$\varepsilon_{\max} = E^*_{\rm CN} - \Delta_{\rm eff} - V_{\rm saddle}(J_{\rm CN}, \eta) - \Delta V_{\rm shell}(J_{\rm CN}, Z_L, A_L). \quad (2)$$

In these expressions, ρ_f is the level density at the saddle point, $\rho_{\rm CN}$ is the level density of the compound nucleus, η denotes the mass asymmetry at the saddle point, and the integration variable ε can be viewed as the kinetic energy of radial motion at the saddle point. As the level density increases rapidly with the effective excitation energy above the saddle point u_J, most of the contributions to the branching ratio arise from smaller values of ε.

Within the transition-state model, it is the phase space at the saddle point, rather than the available number of open channels at scission or in the final fragments, that determines the fission branching ratios. The success of this model in describing the global fission behavior in the ^{32}S+^{24}Mg system [9], as well as in describing the fission behavior for other systems in this mass range [19], supports this assumption. Other models which calculate relative fission probabilities based on the available states at the scission point, such as the extended Hauser Feshbach model [33] and the so-called "Number of Open Channels" model [15,34], can lead to similar results, but only if they are devised in such a way that the phase space at scission mimics that at the saddle point. In any case, the reaction flux must ultimately be distributed among the states of the fragments.

Several simplifying assumptions concerning the energetics in moving from the saddle to scission configurations were used to calculate the excitation-energy spectra. The asymptotic value of the total kinetic energy $E_{K,\rm tot}$ is taken as the sum of the radial component of the kinetic energy at the saddle point ε and the relative potential energy at scission $V_{\rm rel}(\ell_{\rm out}, \eta)$. This relative energy $V_{\rm rel}$, which depends on the orbital angular momentum in the exit channel $\ell_{\rm out}$, can be determined, for example, by approximating the shape of the scission configuration by that of two touching, deformed spheroids [19] and summing their relative nuclear, Coulomb, and rotational energies. Because of the relatively narrow neck in the saddle configuration for light systems, it is generally assumed that the energy difference between the scission and saddle configurations is negligible and, consequently, we have based the scission geometry on the corresponding saddle-point shape [19]. To better reproduce the experimental energy spectra, however, it was found necessary to introduce a parameter δ, which might be viewed as the energy transferred to internal degrees of freedom in moving from the saddle to scission configurations, with the final total kinetic energy given by $E_{K,\rm tot} = V_{\rm rel} + \varepsilon - \delta$. A fixed value of $\delta = 2.5$ MeV was used for all of the calculations reported here.

To calculate the cross sections for populating specific excitations of the fragments, it was first necessary to determine the partial cross section $\sigma_{ff}(J_{\rm CN}, \eta)$ for producing through fusion a compound nucleus of spin $J_{\rm CN}$ that subsequently fissions with a final mass asymmetry η. This was done using the fission widths discussed above within the context of the transition-state model, as discussed in Ref. [19], and with the energetics schematically indicated in Fig. 6. The probability $P(\eta, J_{\rm CN}, \varepsilon)$ for the compound nucleus of spin $J_{\rm CN}$ to fission with mass asymmetry η and radial kinetic energy ε was also determined using the transition-state calculation. The partial cross section $\sigma(\alpha_1, \alpha_2, J_{\rm CN})$ for the compound nucleus at this spin decaying to fragment states α_1 and α_2 is then

$$\sigma(\alpha_1, \alpha_2, J_{\rm CN}) = \sigma_{ff}(J_{\rm CN}, \eta) \frac{\sum_{\ell_{\rm out}} [\alpha_1 \otimes \alpha_2]_{J_{\rm CN}, \ell_{\rm out}} P(\eta, J_{\rm CN}, \varepsilon)}{\sum_{\alpha_1, \alpha_2, \ell_{\rm out}} [\alpha_1 \otimes \alpha_2]_{J_{\rm CN}, \ell_{\rm out}} P(\eta, J_{\rm CN}, \varepsilon)} \quad (3)$$

with the cross section $\sigma(\alpha_1, \alpha_2)$ for populating the mutual excitation $\alpha_1 + \alpha_2$ given by

$$\sigma(\alpha_1, \alpha_2) = \sum_{J_{\rm CN}} \sigma(\alpha_1, \alpha_2, J_{\rm CN}). \quad (4)$$

It should be noted that $P(\eta, J_{\rm CN}, \varepsilon)$ depends implicitly on $\ell_{\rm out}$ through ε. As indicated in Fig. 6, for each mutual excitation $E_x = E_x^{\alpha_1} + E_x^{\alpha_2}$, the energy ε was obtained with

$$\varepsilon = E_{\rm c.m.} + Q_0 - V_{\rm rel}(\ell_{\rm out}, \eta) + \delta - E_x. \quad (5)$$

In principle, one should also expect $V_{\rm rel}$ to depend on the compound nucleus spin, since the shape of the saddle-point configuration depends on this spin. This dependence is not expected to be strong, however, and has been neglected in the present calculation. The spin coupling between the two fragment states and the saddle-point configuration is expressed in terms of the vector-coupling coefficients, with

$$[\alpha_1 \otimes \alpha_2]_{J_{\rm CN}, \ell_{\rm out}} = \sum_s \sum_{m_{s_1}, m_{s_2}, m_\ell} (\langle s_1, m_{s_1}, s_2, m_{s_2}, \mid s, m_s \rangle \langle s, m_s, \ell_{\rm out}, m_\ell \mid J_{\rm CN}, 0 \rangle)^2 \quad (6)$$

and with the summations taken so as to preserve parity. Using the properties of the vector-coupling coefficients, this reduces to a sum over the channel spin values. After finding the predicted cross sections for the mutual excitations of the fragments, it was possible to generate spectra based on these cross sections which could be compared with the experimental results.

IV. DISCUSSION

A. Excitation-energy spectra

In order to compare the calculated excitation-energy spectra with the experimental results, the coincidence efficiencies deduced from the Monte Carlo calculations were used to express the experimental results in terms of differential cross sections $d\sigma/dE$. These spectra are shown in Figs. 7 and 8 for the ^{24}Mg+^{32}S and ^{28}Si+^{28}Si channels, respectively. Based on these spectra, the integrated cross sections for the two channels at the two energies are 2.9 mb and 8.0 mb for ^{24}Mg+^{32}S and 1.9 mb and 5.1 mb for ^{28}Si+^{28}Si at $E_{\text{c.m.}}$=51.0 and 54.5 MeV, respectively. These cross sections are in good agreement with the systematics observed in the earlier singles measurements [9] of this system, where cross sections of 4.0 mb and 10.1 mb for $A_{\text{fragment}} \approx 24$ and 3.0 mb and 13.5 mb for $A_{\text{fragment}} \approx 28$ were found at $E_{\text{c.m.}}$=51.9 and 60.8 MeV, respectively. Differences in the measurements, however, such as the coplanarity condition imposed on the coincidence data, prevent a more exact comparison.

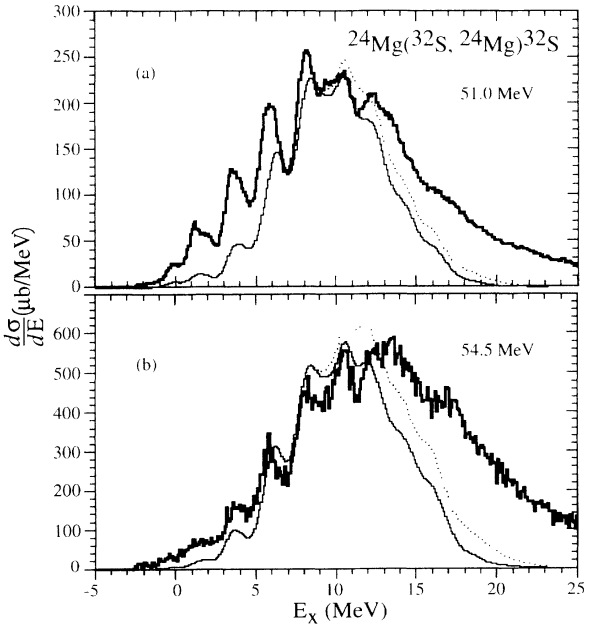

FIG. 7. ^{24}Mg+^{32}S excitation-energy spectra for the ^{32}S+^{24}Mg reaction at (a) $E_{\text{c.m.}}$=51.0 MeV and (b) $E_{\text{c.m.}}$=54.5 MeV. The bold-line histograms are the experimental data. The spectra have been efficiency corrected and normalized according to the Monte Carlo calculations discussed in the text. The lighter curves are the results of the model calculation discussed in the text for fission decay to particle-bound states (solid curve) and for all decays (dotted curve).

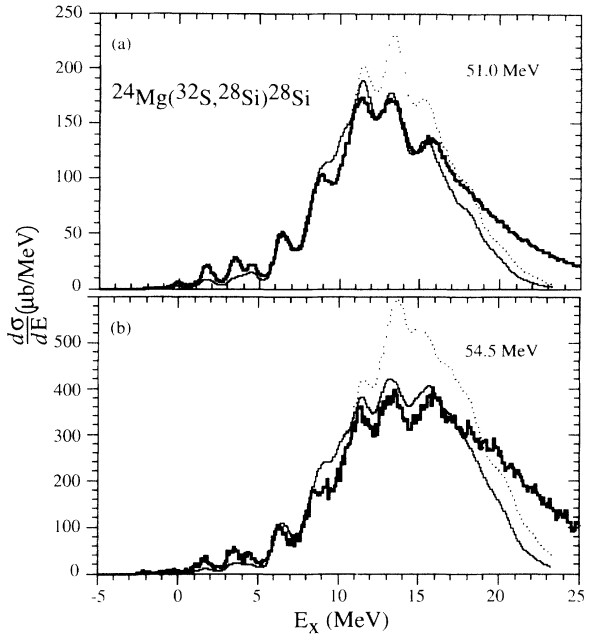

FIG. 8. ^{28}Si+^{28}Si excitation-energy spectra for the ^{32}S+^{24}Mg reaction at (a) $E_{\text{c.m.}}$=51.0 MeV and (b) $E_{\text{c.m.}}$=54.5 MeV. The curves are as discussed for Fig. 7.

The calculated excitation-energy spectra for the ^{24}Mg+^{32}S and ^{28}Si+^{28}Si channels are also shown in Figs. 7 and 8. The parameters used to determine partial cross sections to specific mutual excitations $\sigma(\alpha_1, \alpha_2)$ were the same as those discussed in Ref. [19]. The diffuseness of the fusion ℓ distribution was set to $\Delta = 1\hbar$ and the level density parameters for evaporation-residue and fission decay were set to $a_n = A_{\text{ER}}/(8.0\text{ MeV})$ and $a_f = A_{\text{CN}}/(8.0\text{ MeV})$, respectively. For the two energies, the total fusion cross sections were adjusted to optimize the agreement with the measured cross sections in the symmetric fission channels. The resulting predictions of the evaporation-residue cross sections of 1030 mb and 1065 mb at $E_{\text{c.m.}}$=51.0 and 54.5 MeV, respectively, are in good agreement with the systematics developed for the ^{32}S+^{24}Mg system [9,35]. The only additional parameter introduced for the excitation-energy spectra calculations is the damping parameter δ, for which a value of δ=2.5 MeV was used in all calculations. The level schemes for the ^{24}Mg, ^{28}Si, and ^{32}S nuclei were obtained from the compilation by Endt [36], including levels up to 16.904, 14.339, and 12.488 MeV for the three nuclei, respectively. The limitation imposed on the calculation from the lack of information about states above these energies is somewhat mitigated by the unlikelihood that all of the excitation energy will be deposited in a single fragment during the decay. Both particle-bound and particle-unbound levels were used to determine the excitation-energy division between the fragments but, because of the conditions imposed on the coincidence measurement, the comparison with experiment should primarily involve excita-

tions where both fragments are created in particle-bound states. For comparison with the experimental results, the experimental energy resolutions (Γ_{FWHM}=1.4 MeV and 1.1 MeV for the $^{24}Mg+^{32}S$ and $^{28}Si+^{28}Si$ channels, respectively) were folded into the calculated excitation-energy spectra assuming Gaussian line shapes. Calculated spectra corresponding to particle-bound states only and to both particle-bound and particle-unbound states are shown by the solid and dotted curves in Figs. 7 and 8.

The calculated spectra for particle-bound states are found to reproduce the observed structures in the excitation-energy spectra quite well. In particular, the structures in the excitation-energy range 9–17 MeV of the $^{28}Si+^{28}Si$ channel, where the number of possible mutual excitations is quite large, are in good agreement with experiment. The calculation is less successful in reproducing the yields at higher energies for the two channels, although part of this discrepancy may result from events involving secondary α-particle emission from one of the fragments, in which case the assumptions used in the mass and Q-value calculations fail. Incomplete knowledge of states at high excitation energy in the fragments, particularly high-spin states, may also result in an underestimate of the calculated spectrum at high energies.

High-spin states are particularly significant for two reasons. First, these states have higher statistical weight and are therefore expected to be populated with a greater relative strength. The second consequence of the high-spin states is that they compete for the reaction flux over a wider range of partial waves than low-spin excitations. This can significantly broaden the width of the excitation-energy spectrum, as can be realized by considering the average compound-nucleus spin $\langle J_{CN}\rangle$, the average exit-channel orbital angular momentum $\langle \ell_{out}\rangle$, and the average channel spin $\langle s\rangle$ as a function of the mutual excitation energy. These are shown in Fig. 9 for all mutual excitations of the $^{28}Si+^{28}Si$ channel at $E_{c.m.}$=51 MeV with predicted cross section larger than 1 μb. The range of compound-nucleus spins expected to contribute to the fission cross section in this channel is approximately from 29$\hbar$ to 38$\hbar$. The range of orbital angular momentum, however, is considerably greater, extending from approximately 21$\hbar$ to 38$\hbar$. This behavior, as well as the step function behavior of the average orbital angular momentum, can be understood in terms of the reaction energetics outlined earlier. The exponential behavior of the level densities above the saddle point favors small values of ε. Consequently, for a given value of ℓ_{out}, a specific excitation energy will be favored corresponding to $\varepsilon \rightarrow 0$. The step behavior arises from the discrete nature of the relative angular momentum. Higher excitation energies, which correspond to lower orbital angular momenta, are most easily achieved by an alignment of the orbital angular momentum with a large channel spin.

An alternative explanation for the extent of the excitation-energy spectra is that the partial cross section distribution for fission extends to lower spin values than assumed, as would result if the mass-asymmetry dependence of the fission barrier energy is shallower than expected. The success of the fission calculation in reproducing the fission-mass dependence for this system [9], however, argues against this possibility. A shallower mass dependence of the barrier would also lead to a less asymmetric mass distribution than observed.

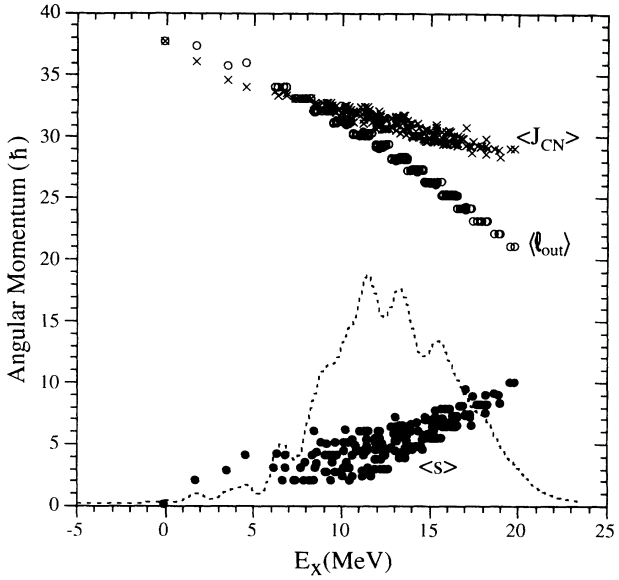

FIG. 9. Average calculated values for the compound-nucleus spin $\langle J_{CN}\rangle$, exit-channel orbital angular momentum $\langle \ell_{out}\rangle$, and channel spin $\langle s\rangle$ for the $^{32}S+^{24}Mg \rightarrow ^{56}Ni^* \rightarrow ^{28}Si^* + ^{28}Si^*$ fusion-fission reaction at $E_{c.m.}$=51.0 MeV. The calculated excitation-energy spectrum for particle-bound states is overlaid for orientation purposes (scale not shown).

There is an intriguing suggestion in Fig. 9 that the statistical phase space might favor an anti-aligned configuration of the orbital angular momentum and channel spin at lower excitation energies, with $\langle \ell_{out}\rangle$ greater than $\langle J_{CN}\rangle$. A test of this possibility will require a spin alignment measurement of the low-lying excitations, as has been done by Wuosmaa *et al.* [31,37] in the $^{24}Mg+^{24}Mg$ system. Unfortunately, the low cross sections for these channels makes such measurements very difficult. The cross section for the $^{28}Si_{g.s.}+^{28}Si_{g.s.}$ channel at $E_{c.m.}$=51 MeV, for example, is $\approx$5.7 μb, based on the analysis presented in the next section. The calculated preferential feeding of an anti-aligned configuration would also vanish if the tail of the fusion partial cross section distribution were allowed to extend to higher spin values. Evidence supporting the assumed partial cross section distribution is found, however, in the measured angular distribution for ground-state population of fragments in the $^{28}Si+^{28}Si$ channel, as discussed in the next section.

B. Angular distribution for $^{24}Mg(^{32}S,^{28}Si_{g.s.})^{28}Si_{g.s.}$ reaction at $E_{c.m.}$=51 MeV

The $^{24}Mg(^{32}S,^{28}Si_{g.s.})^{28}Si_{g.s.}$ spinless, identical-particle exit channel at $E_{c.m.}$=51 MeV was found to have a strongly oscillatory angular distribution, as shown in Fig. 10. This behavior can be understood if the distribution is dominated by a single partial wave, or

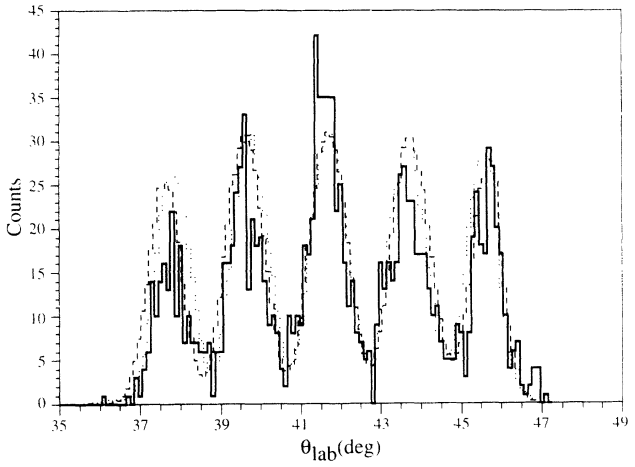

FIG. 10. Experimental angular distribution for the ^{24}Mg(^{32}S, ^{28}Si$_{g.s.}$)^{28}Si$_{g.s.}$ reaction at $E_{c.m.}$=51 MeV (solid histogram). Calculated distributions based on a $\mid P_\ell(\cos\theta_{c.m.}) \mid^2$ angular dependence folded with the detection efficiency, as discussed in the text, are shown for $\ell = 38\hbar$ (dashed histogram) and $\ell = 40\hbar$ (dotted histogram).

by a few partial waves that are in phase, leading to a $\mid P_\ell(\cos\theta_{c.m.}) \mid^2$ angular dependence. To determine the dominant ℓ value for this distribution, the previously discussed Monte Carlo calculation of the experimental response was modified to use a $\mid P_\ell(\cos\theta_{c.m.}) \mid^2$ angular dependence, corresponding to a single partial wave, for the ^{28}Si$_{g.s.}$+^{28}Si$_{g.s.}$ breakup channel. The resulting laboratory distributions for $\ell = 38\hbar$ and $40\hbar$ are shown by the dashed and dotted distributions in Fig. 10. Although the best reproduction of the experimental distribution is found assuming $\ell = 40\hbar$, either angular momentum is seen to be consistent with the data.

The calculated average angular momentum for the symmetric-fragment ground-state decay is seen from Fig. 9 to be about $38\hbar$. This value is in good agreement with the angular distribution measurement and supports the diffuseness assumed for the fusion ℓ distribution in the analysis. The observed angular momentum is also comparable with, or somewhat larger than, the grazing angular momentum in either the ^{32}S+^{24}Mg entrance channel ($\ell_g \approx 35\hbar$) or the ^{28}Si+^{28}Si exit channel ($\ell_g \approx 38\hbar$), again highlighting the large deformation associated with the fission saddle point.

The reduced counting statistics for the $E_{c.m.}$=54.5 MeV data prevent a similar analysis for those data. Also, the data for the ^{24}Mg$_{g.s.}$+^{32}S$_{g.s.}$ channel at $E_{c.m.}$=51 MeV show much less structure than observed for the symmetric-mass breakup channel, suggesting a more complicated interference of the participating partial waves. The apparent simplicity of the ^{28}Si$_{g.s.}$+^{28}Si$_{g.s.}$ distribution may reflect the identical-particle nature of this channel where only the even partial waves contribute.

C. Comparison with the ^{28}Si(^{28}Si,^{28}Si)^{28}Si reaction

It is interesting to compare the ^{32}S(^{24}Mg,^{28}Si)^{28}Si results to those reported earlier by Betts *et al.* [20,28,29] for the large-angle scattering yields of the ^{28}Si(^{28}Si,^{28}Si)^{28}Si reaction. In those ^{28}Si+^{28}Si entrance-channel measurements, strong resonance behavior was observed in excitation functions for the low-lying elastic and inelastic channels. In Fig. 11(a), we show the energy spectrum obtained at $E_{c.m.}$=60 MeV by detecting the outgoing fragments in coincidence using two position-sensitive, Si (surface-barrier) detectors [30]. The measurement was performed using thin ^{28}Si foils and, consequently, had excellent energy resolution. To compare the fission calculations for the ^{28}Si+^{28}Si entrance channel with the experimental results, the original spectrum of Ref. [30] has been efficiency corrected based on the geometry of this measurement, as discussed in Ref. [28]. (The experimental efficiency is calculated to have changed by approximately 25% over the range 0 MeV$\leq E_x \leq$ 22 MeV.) Although the efficiency-adjusted data have not been converted to cross sections, the scale of Fig. 11(a) has been adjusted using the experimental cross sections for low-lying excitations [38] to allow comparison with the model calculation shown in Fig. 11(b). The resonant nature of this reaction leads to an uncertainty as large as 50% in this scaling procedure, but the qualitative comparison of the experimental and calculated spectra should still remain valid. The model calculation uses the same assumptions as discussed for the ^{32}S+^{24}Mg system.

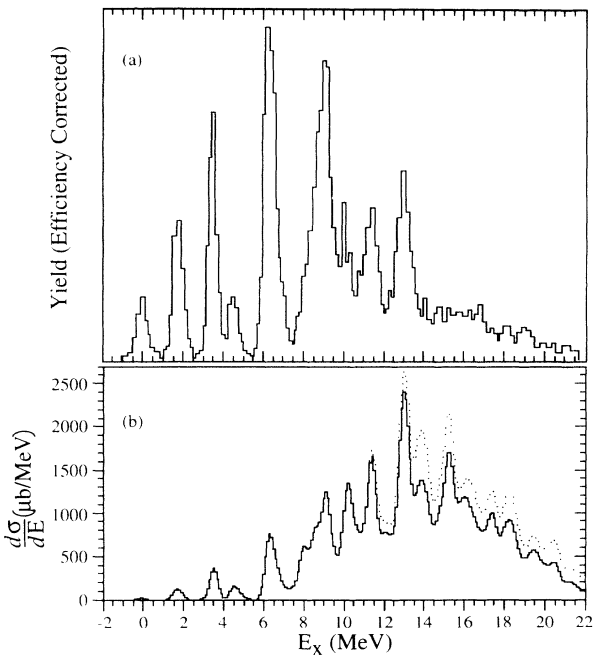

FIG. 11. (a) Excitation-energy spectrum obtained by Betts *et al.* [28] for the ^{28}Si(^{28}Si, ^{28}Si)^{28}Si reaction at $E_{c.m.}$= 60 MeV. The data have been efficiency corrected and the ordinate has been scaled to allow for the calculated results, shown in part (b), to be compared with the data. No scale is shown because of the large normalization uncertainty, as discussed in the text. (b) Calculated excitation-energy spectra based on the fission-model calculation. The solid curve is for decays that populate two particle-bound fragment states. The dotted curve includes all decays.

The only reaction-dependent change (other than specification of the entrance channel) is the assumption of a total fusion cross section of 1250 mb, leading to a calculated evaporation-residue cross section at this energy of 1030 mb (to be compared with the experimental value of 1040±32 mb of DiCenzo *et al.* [39]).

It is evident from Fig. 11 that while the fission model calculation is able to describe the more fully damped cross sections for the ^{28}Si+^{28}Si reaction, including the structure observed with E_x >10 MeV, the model greatly underpredicts the strength observed in the low-lying states. The strong resonance behavior observed in the energy dependence of these excitations suggests that a separate mechanism, in addition to the fusion-fission process, contributes to these yields. Angular distributions for the ^{28}Si(^{28}Si,^{28}Si$_{g.s.}$)^{28}Si$_{g.s.}$ reaction at $E_{c.m.}$=59 MeV and 64 MeV indicate dominant ℓ values of 40$\hbar$ and 42$\hbar$, respectively [28]. The calculated average angular momentum leading to fission to the ground state at $E_{c.m.}$=60 MeV is 42.4$\hbar$, suggesting competition between the fission and resonance reaction mechanism. Betts *et al.* [20,21,30] have noted that when shell corrections are applied to the liquid-drop potential-energy surface for ^{56}Ni, there is a significant second minimum found just inside the fission barrier for $J = 40\hbar$. The present results suggest that the observed excitation spectrum may be the consequence of fission from high-spin shape isomers in ^{56}Ni, as previously suggested, which dominates the lower excitations, together with the statistical fission of the "normal" compound nucleus, which plays a greater role for the higher energy excitations.

D. γ-ray yields

Based on the particle data, it is impossible to assign specific mutual excitations to the structures observed in the excitation-energy spectra of Figs. 7, 8, and 11 at higher energies. This is seen in Fig. 12, where the calculated cross sections for different mutual excitations are shown as functions of excitation energy for the ^{24}Mg(^{32}S,^{24}Mg)^{32}S [Fig. 12(a)] and ^{24}Mg(^{32}S,^{28}Si)^{28}Si [Fig. 12(b)] reactions at $E_{c.m.}$=51 MeV, and for the ^{28}Si(^{28}Si,^{28}Si)^{28}Si [Fig. 12(c)] reaction at $E_{c.m.}$=60 MeV. The experimental spectra are overlaid for orientation purposes. At energies above ≈6.5 MeV, a number of different mutual excitations can contribute to each of the observed structures in these spectra, and the calculations indeed suggest that groupings at certain energies of a number of high-spin excitations contribute to these structures. The total number of mutual excitations of particle-bound states for each MeV of excitation energy is also shown in Fig. 12 for the different reactions. Although this number becomes quite large above 10 MeV, the dominance of less common high-spin excitations results in significant structure. The need for great caution in suggesting a specific excitation for one of the higher energy peaks is obvious.

The complexity of the higher energy structures is also apparent in the γ-ray spectra obtained in coincidence with the particle data for the ^{24}Mg(^{32}S,^{28}Si)^{28}Si reaction at $E_{c.m.}$=51 MeV. With the modest energy resolution of this experiment, the peak in Fig. 8(a) that appears to correspond to the single 4^+ excitation at 4.617 MeV is already found to have a significant cross section component coming from the excited 0^+ state at 4.979 MeV. This conclusion is reached from the detailed study of the γ-ray spectra. By gating on the energy range 4.3 MeV$\leq E_x \leq$ 5.4 MeV in the particle spectrum, the γ-ray yields for the $2^+_{1779} \rightarrow 0^+_{g.s.}$, $4^+_{4617} \rightarrow 2^+_{1779}$, and $0^+_{4980} \rightarrow 2^+_{1779}$ transitions are found to be 15, 7, and 3 counts, respectively. After correction for the absolute efficiencies for the three transitions 2.43×10^{-3}, 1.71×10^{-3}, and 1.55×10^{-3}, the total number of events corresponding to each transition are 6175, 4096, and 1930, respectively. The total number of events feeding the 2^+ level is then 6026, in good agreement with the number of decays from this state. The γ-ray analysis indicates that 68% of the yield within the indicated excitation-energy window corresponds to the 4^+ excitation, with 32% arising from the excited 0^+

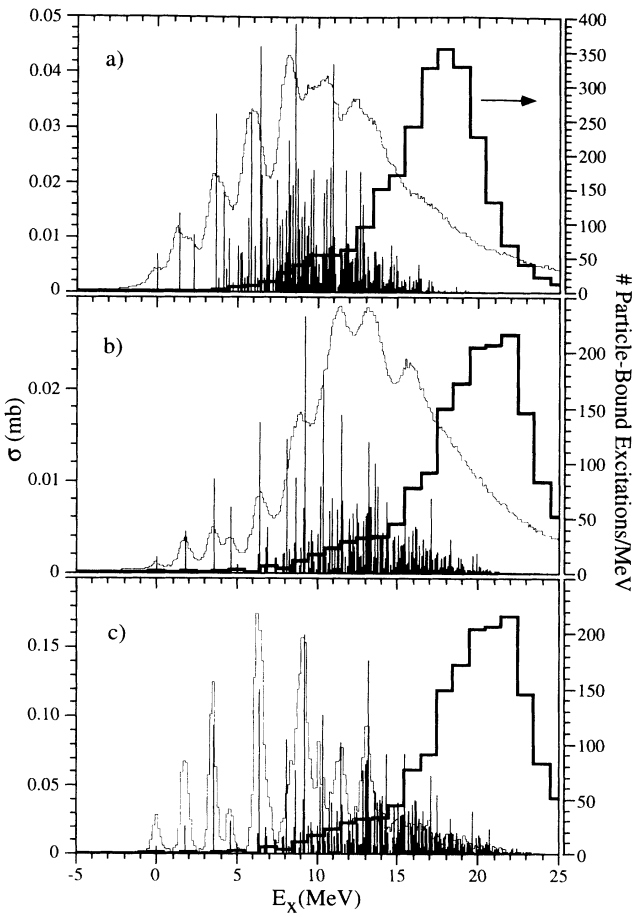

FIG. 12. Calculated fission cross sections (vertical lines) for single and mutual excitations in the (a) ^{24}Mg(^{32}S, ^{24}Mg)^{32}S reaction at $E_{c.m.}$=51 MeV, (b) ^{24}Mg(^{32}S,^{28}Si)^{28}Si reaction at $E_{c.m.}$= 51 MeV, and (c) ^{28}Si(^{28}Si,^{28}Si)^{28}Si reaction at $E_{c.m.}$=60 MeV. The corresponding experimental excitation-energy spectra have been overlaid for orientation purposes (thin-line histograms; scale not shown). The total number of excitations corresponding to fission decay to particle-bound fragments per MeV is shown by the bold histogram (use ordinate scale at right).

state. Although there is a large statistical uncertainty in the $4^+_{4617}/0^+_{4980}$ yield ratio, a significant 0^+ component is clearly indicated. The calculated cross section percentages for these two single excitations are 90% (4^+) and 10% (0^+).

It is worth noting that, in the data of Betts *et al.* [30] for the ^{28}Si(^{28}Si,^{28}Si)^{28}Si reaction, there is a small shoulder on the peak centered at 4.617 MeV that could indicate population of the excited 0^+ state. However, this shoulder is considerably less than expected based on the calculation for this reaction where a ratio of $4^+_{4618}/0^+_{4979} = 4/1$ is predicted. This is consistent with the suggestion that resonant yields in this reaction result primarily from excitations of the yrast levels [28].

The next peak in the excitation-energy spectrum is centered near the yrast $2^+_{1779} + 4^+_{4617}$ mutual excitation at 6.396 MeV. Based solely on the particle spectrum, one could be tempted to assign this peak entirely to the mutual excitation of yrast states. Analysis of the γ-ray spectrum corresponding to the excitation-energy range 5.9 MeV$\leq E_x \leq$ 7.3 MeV, however, suggests a more complicated picture. There are five additional single and mutual excitations within $\pm$0.5 MeV of the $2^+_{1779} + 4^+_{4617}$ excitation. To determine the fraction of the yield resulting from these excitations, we used the γ-ray data obtained *both* with the Ge and with the BGO detectors. Although the limited energy resolution of the BGO detectors generally restricts their usefulness in determining the population of different levels, in this case there are relatively few excitations involved, and the data proved valuable in deducing the relative population of the 3^-_{6879} and 4^+_{6888} excitations. The 4^+_{6888} state has a 100% decay branch to the 2^+_{1779} level. The corresponding 5109 keV γ ray is unresolved in the spectra from the 5100 keV line arising from the 30% $3^-_{6879} \rightarrow 2^+_{1779}$ transition. The 3^- level also has a 70% branch to the ground state, but the high energy of this γ ray leads to a low detection efficiency in the Ge detectors. Within the energy-gated spectrum, there were three γ rays within the region of the 5100/5109 keV doublet and no γ rays observed at 6879 keV ($3^-_{6879} \rightarrow 0^+_{g.s.}$). However, this higher-energy transition was clearly seen in the spectrum obtained by taking the logical *or* of the individual BGO spectra, with 483 counts observed. Using these data it was possible to deduce the relative contribution of the 6.879 MeV and 6.888 MeV levels. By deriving a population scheme consistent with both the high-resolution Ge and the BGO data, we deduce the following percent populations for the excitations within this energy range, giving the experimental population followed by the calculated value: 3^+_{6276}(<5%; 6%), $2^+_{1779} + 4^+_{4617}$ (46%; 53%), 0^+_{6691} (10%; 3%), $2^+_{1779} + 0^+_{4979}$(15%; 8%), 3^-_{6879} (18%; 13%), 4^+_{6888} (11%; 16%). Although the calculated percentages are in reasonably good agreement with the experimental values, the underprediction of the 0^+_{6691} excitation is interesting, since a similar trend is also found at higher energies where the population of members of the strongly prolate deformed band with the 0^+_{6691} level as the suggested bandhead are consistently underestimated in the calculations.

The very weak population of the collective 3^-_{6879} excitation in the ^{28}Si(^{28}Si,^{28}Si)^{28}Si reaction data has been noted by Betts *et al.* [28] as one of the significant features of these data. The significant population of this excitation in the ^{24}Mg(^{32}S,^{28}Si)^{28}Si reaction is then further evidence that quite different reaction mechanisms dominate the low-lying excitations for the two entrance channels.

For energies with $E_x > 7.5$ MeV, the large number of possible mutual excitations within the experimental resolution of a given energy peak, and the complexity of the γ-ray spectra found by gating on one of these peaks, made it impossible to uniquely determine the relative population of the different excitations. It is still possible, however, to compare more generally the fission model calculation with the experimental results even at these energies. For this comparison, the relative cross sections calculated for the mutual excitations of the ^{24}Mg(^{32}S,^{28}Si)^{28}Si reaction at $E_{c.m.}$=51 MeV, as shown in Fig. 12(b), were used to generate a model γ-ray spectrum corresponding to an excitation-energy range of 7.6$\leq E_x \leq$16.7 MeV. Within this range the calculated excitation-energy spectrum, shown in Fig. 8(a), is in very good agreement with experiment, and the comparison of calculated and measured γ-ray spectra should be meaningful. The calculated γ-ray spectrum is based on the measured branching ratios for the γ-decaying states of ^{28}Si and takes into account the Ge detection efficiency. The total number of symmetric fission events assumed in generating this spectrum was taken as the measured yield in this energy range, reduced by 10% in order to take into account instances where different fission channels are involved or where secondary light-fragment emission occurred from one of the primary ^{28}Si fission fragments. This correction was based on the strength of the lines corresponding to these processes observed in the γ-ray spectrum. It is assumed that the large angular range of the particle detectors and the range of angles covered by the Ge detectors is sufficient to minimize any effects associated with angular correlation of the emitted γ rays.

The experimental excitation-energy-gated γ-ray spectrum is shown full scale in Fig. 13(a) and with an expanded scale in Fig. 14(a). A smooth background has been subtracted to facilitate comparison of the corresponding calculated spectra, shown in Figs. 13(b) and 14(b), with these results. The various peaks in the calculated spectrum have been folded with Gaussian distributions of the same width as the experimental detector and Doppler-broadening response. From Fig. 13 we find that the decay strength from the yrast 2^+ and 4^+ levels are well accounted for by the calculation. Since most of the decay strength of ^{28}Si passes through the 2^+_{1779} level, the success in reproducing this strength is primarily a check on the total number of ^{28}Si fragments assumed in the calculation. The success in reproducing the strength of the $4^+_{4618} \rightarrow 2^+_{1779}$ transition is more interesting, since the 4^+ level is primarily fed by transitions from higher spin, positive-parity transitions. As previously indicated, the model calculation favors the population of high-spin states in this excitation-energy range, and so this agreement supports this feature of the calculation.

Closer inspection of the transition strengths, as shown

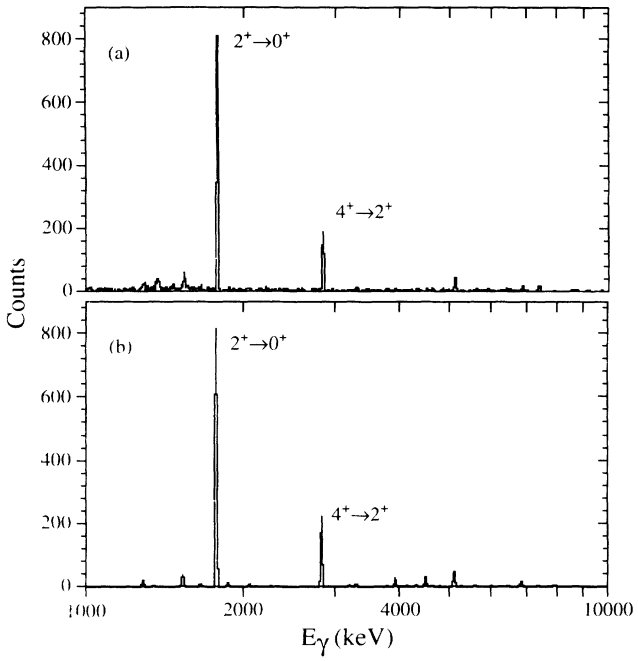

FIG. 13. (a) Experimental and (b) Calculated γ-ray spectra for the ^{24}Mg(^{32}S,^{28}Si)^{28}Si reaction at $E_{c.m.}$=51.0 MeV with 7.6 MeV$\leq E_x \leq$16.7 MeV. A smooth background has been subtracted from the experimental yields for this comparison.

in Fig. 14 where the stronger transitions are labeled, reveals some interesting differences between the calculated and experimental results. The observed strength for the $6^+_{8543} \rightarrow 4^+_{4618}$ transition within the ground-state band, for example, is considerably weaker than calculated. This indicates that the yrast band does not have any special significance in producing the structures at higher energies in the excitation-energy spectrum. Based solely on an excitation energy measurement, the peak near $E_x \approx$ 13.2 MeV might be attributed to the mutual $4^+_{4618}+6^+_{8543}$ excitation. The γ-ray data show that this is not the case. (Gating more narrowly on the excitation-energy peak near 13.2 MeV, we observe only 7±4 γ rays corresponding to the $6^+_{8543} \rightarrow 4^+_{4618}$ transition. If the net yield associated with this peak of 28 300 counts is attributed to the $4^+_{4618} + 6^+_{8543}$ mutual excitation, we would expect to observe $\approx$37 γ rays for the $6^+_{8543} \rightarrow 4^+_{4618}$ transition.)

The calculated and experimental transition yields are compared in Fig. 15. The level scheme of ^{28}Si, as proposed by Glatz *et al.* [40–42], is shown at the top of this figure. The branching ratios for the stronger transitions are indicated. At the bottom of the figure is a plot of the calculated γ-ray yield for the different transitions (open diamonds) and the corresponding experimental values (indicated as uncertainty ranges). To help in associating the yields with specific transitions, the associated branching ratios are also indicated in the plot of the yields.

In general the calculated and experimental yields are in good agreement. Other than for the $6^+_{8543} \rightarrow 4^+_{4618}$ transition, the only significant overprediction of the transition strength is for the $3^+_{6276} \rightarrow 2^+_{1779}$ decay. The predicted strengths for the other members of the $K^\pi = 3^+$ band also tend to be somewhat larger than observed, but are still within the range of the experimental uncertainties. The negative-parity bands and the first excited $K^\pi = 0^+$ are also well described by the calculation.

The transition strengths for the 0^+_{6691}, 4^+_{9165}, and 6^+_{11509} members of the second excited $K^\pi = 0^+$ are, however, significantly underpredicted by the calculation. This

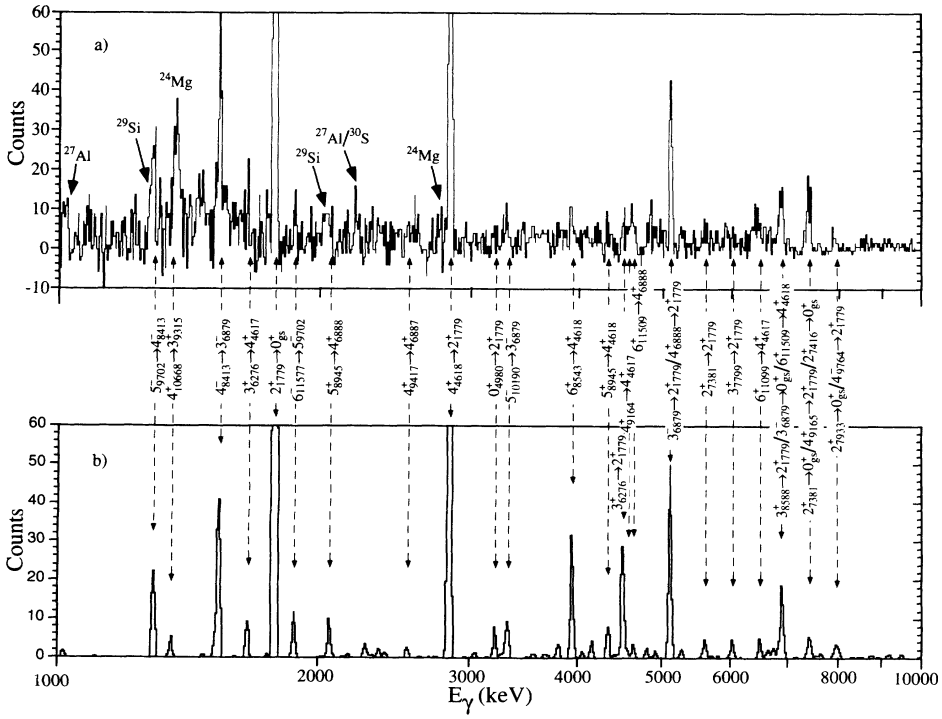

FIG. 14. Same as Fig. 13, except with an expanded scale.

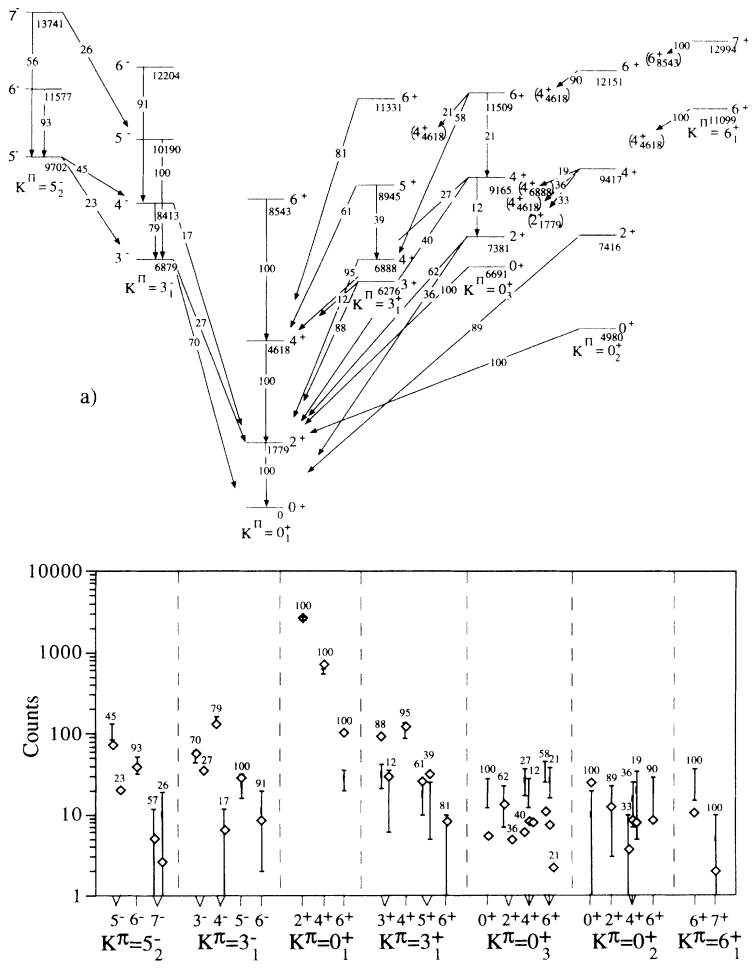

FIG. 15. (a) Band structure of ^{28}Si as suggested by Glatz *et al.* [40–42] (b) Observed (error ranges) and calculated (open diamonds) transition strengths for states in ^{28}Si populated in the ^{24}Mg+^{32}S fusion-fission reaction at $E_{c.m.}$=51.0 MeV and with 7.6 MeV$\leq E_x \leq$16.7 MeV. The corresponding branching ratios are shown to help in identifying particular transitions.

band has been interpreted as being associated with a large prolate deformation [40]. Its strong population in the fission process might then be understood in terms of the similarity between this prolate shape and the shape of the scission-point configuration. It should be noted that the 0^+_{6691}, 2^+_{7381}, and 4^+_{9165} members of this band have been found to be strongly populated in a ^{16}O+^{12}C radiative capture experiment, supporting the claim of a large prolate-intrinsic shape. However, the 6^+_{11509} state is not observed in this capture measurement and, as a result, there is some doubt about its association with the prolate band [43]. Regardless of the structure of the 6^+_{11509} state, further evidence of the importance of the nuclear structure at scission on the population of fragment states is seen by comparing the measured strengths of the 6^+_{11331} and 6^+_{11509} levels. These two states are very close in energy and they are both likely to be fed directly in the fission process rather than in decays from higher-lying levels. By taking the number of observed γ rays associated with the decay from these levels and dividing by the product of the transition branching ratio and the Ge efficiency, it is possible to deduce the total number of particle events corresponding to the population of these levels. For the 6^+_{11331} level, there is no indication of a γ-ray peak corresponding to the $6^+_{11331} \rightarrow 4^+_{4618}$ transition (81% branch). This places the upper limit on the total number of events feeding this level at $\approx$20000. Alternatively, 35$\pm$10 γ rays from the $6^+_{11509} \rightarrow 4^+_{6888}$ transition and 27$\pm$11 γ rays from the $6^+_{11509} \rightarrow 4^+_{9165}$ transition are observed, corresponding to a weighted particle yield of 59200$\pm$14000. Thus the single 6^+_{11509} excitation and the 2^+_{1779} + 6^+_{11509} mutual excitation are seen to be significant contributors to the peaks observed in the excitation-energy spectra near the corresponding energies.

V. SUMMARY AND CONCLUSIONS

The symmetric fission of ^{56}Ni has been studied using the ^{32}S+^{24}Mg reaction at $E_{c.m.}$=51.0 and 54.5 MeV. Excitation-energy spectra for the ^{24}Mg+^{32}S and ^{28}Si+^{28}Si fission channels have been measured using a particle-particle coincidence technique. Structure is observed in these spectra to high excitation energies where the number of possible mutual excitations becomes quite large. For each channel, these structures are found to be common at the two energies.

A simple model calculation is developed to describe the observed excitation spectra. This calculation extends a previously developed fusion-fission model based on the transition state picture. The earlier calculations have been found to successfully reproduce fission cross sec-

tions, mass distributions, and average kinetic energies for light nuclear systems. The model extension involves following the fission decay from the saddle point to individual excitations in the fragments, assuming a statistical weighting of the fragment states. The ability of the newer model calculations to reproduce the structure observed in the excitation-energy spectra suggests that at higher energies these structures are primarily a consequence of the grouping in energy of several high-spin, mutual excitations.

Support for the compound-nucleus partial cross section distribution assumed in the model calculation is found in a measurement of the $^{28}Si_{g.s.}+^{28}Si_{g.s.}$ angular distribution at $E_{c.m.}$=51 MeV. This distribution is found to have a $|\ P_\ell(\cos\theta_{c.m.})\ |^2$ angular dependence characterized by an angular momentum of $\approx 40\hbar$, in good agreement with the average angular momentum expected for ground-state fission of $38\hbar$.

In comparing the calculated cross sections for the symmetric $^{28}Si+^{28}Si$ fission channel resulting from the $^{28}Si+^{28}Si$ reaction at $E_{c.m.}$=60 MeV to the corresponding measurements of Betts *et al.* [20,21,28–30], it is found that the calculation is able to reproduce the behavior of the excitation-energy spectrum at higher energy, but significantly underestimates the cross section for the low-lying states. This result is consistent with a separate mechanism, presumably that responsible for the heavy-ion resonance behavior, dominating the low-energy yields. The dominant angular momentum that has been deduced for the elastic scattering at larger angles, however, is in good agreement with the fission-model calculations. This suggests that the shape of the resonance configuration may be very similar to that of the nuclear saddle point.

The γ rays associated with the symmetric-mass fission channel have also been measured for the $^{32}S+^{24}Mg$ reaction at $E_{c.m.}$=51 MeV. The analysis of these data supports the results of the model calculation, suggesting that the structures observed at higher energies in the excitation spectra arise from groupings of high-spin excitations. *The γ-ray data also indicate, however, that the fission decay is not solely determined by statistical spin factors. In particular, there is evidence of an enhanced role for a highly deformed prolate band in ^{28}Si.* The structure of the nucleus at scission is seen to have a significant influence on the details of the fission decay.

This work concentrates on a system where the fully energy-damped yields have been found, from previous measurements, to be well described by the fusion-fission mechanism. By developing the systematics and a more general understanding of the population of specific states in fission fragments, we hope to learn more about the role of nuclear structure in the fission decay process. This should also help in developing the differences and possible relationships between the heavy-ion resonance and compound-nucleus fission processes in light systems.

ACKNOWLEDGMENTS

This work was supported by the U.S. Department of Energy, Nuclear Physics Division, under Contracts No. DE-FG02-89ER40506 and No. W-31-109-ENG-38. Additional support has come from the University of Kansas General Research Fund.

[1] D. Shapira, J.L.C. Ford, Jr., J.G. del Campo, R.G. Stokstad, and R.M. DeVries, Phys. Rev. Lett. **43**, 1781 (1979).

[2] D. Shapira, R. Novotny, Y.D. Chan, K.A. Erb, J.L.C. Ford, Jr., J.C. Peng, and J.D. Moses, Phys. Lett. **114B**, 111 (1982).

[3] K. Grotowski, Z. Majka, R. Płaneta, M. Szczodrak, Y. Chan, G. Guarino, L.G. Moretto, D.J. Morrissey, L.G. Sobotka, R.G. Stokstad, I. Tserruya, S. Wald, and G.J. Wozniak, Phys. Rev. C **30**, 1214 (1984).

[4] R. Ritzka, W. Dünnweber, A. Glaesner, W. Hering, H. Puchta, and W. Trautmann, Phys. Rev. C **31**, 133 (1985).

[5] A. Ray, S. Gil, M. Khandaker, D.D. Leach, D.K. Lock, and R. Vandenbosch, Phys. Rev. C **31**, 1573 (1985).

[6] A. Ray, D.D. Leach, R. Vandenbosch, K.T. Lesko, and D. Shapira, Phys. Rev. Lett. **57**, 815 (1986).

[7] S.J. Sanders, R.R. Betts, I. Ahmad, K.T. Lesko, S. Saini, B.D. Wilkins, F. Videbaek, and B.K. Dichter, Phys. Rev. C **34**, 1746 (1986).

[8] S.J. Sanders, D.G. Kovar, B.B. Back, C. Beck, B.K. Dichter, D. Henderson, R.V.F. Janssens, J.G. Keller, S. Kaufman, T.-F. Wang, B. Wilkins, and F. Videbaek, Phys. Rev. Lett. **59**, 2856 (1987).

[9] S.J. Sanders, D.G. Kovar, B.B. Back, C. Beck, D.J. Henderson, R.V.F. Janssens, T.F. Wang, and B.D. Wilkins, Phys. Rev. C **40**, 2091 (1989).

[10] A. Szanto de Toledo, M.M. Coimbra, N. Added, R.M. Anjos, N. Carlin Filho, L. Fante Jr., M.C.S. Figueira, V. Guimarães, and E.M. Szanto, Phys. Rev. Lett. **62**, 1255 (1989).

[11] C. Beck, B. Djerroud, B. Heusch, R. Dayras, R.M. Freeman, F. Haas, A. Hachem, J.P. Wieleczko, and M. Youlal, Z. Phys. A **334**, 521 (1989).

[12] S. Cavallaro, Y.S. Zhi, G. Prete, and G. Viesti, Phys. Rev. C **40**, 98 (1989).

[13] S.J. Sanders, B.B. Back, R.V.F. Janssens, D.G. Kovar, D. Habs, D. Henderson, T.-L. Khoo, H. Korner, G. Rathke, T.F. Wang, and F.L.H. Wolfs, Phys. Rev. C **41**, 1901 (1990).

[14] A. Ray, D. Shapira, J. Gomez del Campo, H.J. Kim, C. Beck, B. Djerroud, B. Heusch, D. Blumenthal, and B. Shivakumar, Phys. Rev. C **44**, 514 (1991).

[15] C. Beck, B. Djerroud, F. Haas, R.M. Freeman, A. Hachem, B. Heusch, A. Morsad, M. Youlal, Y. Abe, A. Dayras, J.P. Wieleczko, T. Matsuse, and S.M. Lee, Z. fur Physik **A343**, 309 (1992).

[16] C. Beck, B. Djerroud, F. Haas, R.M. Freeman, A. Hachem, B. Heusch, A. Morsad, M. Vuillet-A-Cilles, and S.J. Sanders, Phys. Rev. C **47**, 2093 (1993).

[17] B. Shivakumar, S. Ayik, B.A. Harmon, and D. Shapira, Phys. Rev. C **35**, 1730 (1987).

[18] A. Lépine-Szily, J.M. Oliveira Jr., P. Fachini, R. Lichenthaler Filho, M.M. Obuti, W. Sciani, M.K. Steinmayer,

and A.C.C. Villari, Nucl. Phys. **A539**, 487 (1992).
[19] S.J. Sanders, Phys. Rev. C **44**, 2676 (1991).
[20] R.R. Betts, B.B. Back, and B.G. Glagola, Phys. Rev. Lett. **47**, 23 (1981).
[21] R.R. Betts and S. Saini, Physica Scripta **T5**, 204 (1983).
[22] R.W. Zurmühle, P. Kutt, R.R. Betts, S. Saini, F. Haas, and O. Hansen, Phys. Lett. **129B**, 384 (1983).
[23] U. Abbondanno, F. Demanins, P. Boccaccio, L. Vannucci, R.A. Ricci, G. Vannini, and N. Cindro, Il Nuovo Cimento (Note Brevi) **97A**, 205 (1987).
[24] A.T. Hasan, S.J. Sanders, K.A. Farrar, F.W. Prosser, B.B. Back, R.R. Betts, M. Freer, D.J. Henderson, R.V.F. Janssens, A.H. Wuosmaa, and A. Szanto de Toledo, Phys. Rev. C **49**, 3 (1994).
[25] R.V.F. Janssens, T.L. Khoo, E. Funk, U. Garg, J. Kolata, and J. Mihelich, *A Proposal for a BGO Sum-Energy/Multiplicity Spectrometer and Multi-Compton Suppression Spectrometer System* (Argonne National Laboratory, Argonne, IL).
[26] F.L.H. Wolfs, Phys. Rev. C **36**, 1379 (1987).
[27] G.F. Knoll, *Radiation Detection and Measurement* (Wiley, New York, 1979).
[28] R.R. Betts, H.-G. Clerc, B.B. Back, I. Ahmad, K.L. Wolf, and B.G. Glagola, Phys. Rev. Lett. **46**, 313 (1981).
[29] R.R. Betts, S.B. DiCenzo, and J.F. Peterson, Phys. Lett. **100B**, 117 (1981).
[30] R.R. Betts, in *Proceedings of the 5th Adriatic International Conference on Nuclear Physics*, edited by N. Cindro, W. Greiner, and R. Caplar (World Scientific, Singapore, 1984) p. 33.
[31] A.H. Wuosmaa, R.W. Zurmühle, P.H. Kutt, S.F. Pate, S. Saini, M.L. Halbert, and D.C. Hensley, Phys. Rev. C **41**, 2666 (1990).
[32] F. Pühlhofer, Nucl. Phys. **A280**, 267 (1977).
[33] T. Matsuse and S.M. Lee, in *Proceedings of the Developments of Nuclear Cluster Dynamics*, edited by Y. Akaishi, K. Kato, H. Noto, and S. Okabe (World Scientific, Singapore, 1988) p. 312.
[34] F. Haas and Y. Abe, Phys. Rev. Lett. **46**, 1667 (1981).
[35] D.G. Kovar, in *Proceedings of the IPCR Symposium on Macroscopic Features of Heavy-ion Collisions and Preequilibrium Process*, edited by H. Kamitsubo and M. Ishihara (Hakone, Japan, 1977) p. 18.
[36] P.M. Endt, Nucl. Phys. **A521**, 1 (1990).
[37] A.H. Wuosmaa, R.W. Zurmühle, P.H. Kutt, S.F. Pate, S. Saini, M.L. Halbert, and D.C. Hensley, Phys. Rev. Lett. **58**, 1312 (1987).
[38] R.R. Betts, Comments Nucl. Part. Phys. **13**, 61 (1984).
[39] S.B. DiCenzo, J.F. Petersen, and R.R. Betts, Phys. Rev. C **23**, 2561 (1981).
[40] F. Glatz, P. Betz, J. Siefert, F. Heidinger, and H. Röpke, Phys. Rev. Lett. **46**, 1559 (1981).
[41] F. Glatz, J. Siefert, P. Betz, E. Bitterwolf, A. Burkard, F. Heidinger, T. Kern, R. Lehmann, S. Norbert, and H. Röpke, Z. Phys. A **303**, 239 (1981).
[42] F. Glatz, M. Lickert, A. Burkard, T. Kern, R. Lehmann, S. Norbert, H. Röpke, J. Siefert, and B.H. Wildenthal, Z. Phys. A **324**, 173 (1986).
[43] M.T. Collins, A.M. Sandorfi, D.H. Hoffmann, and M.K. Salomaa, Phys. Rev. Lett. **49**, 1553 (1982).

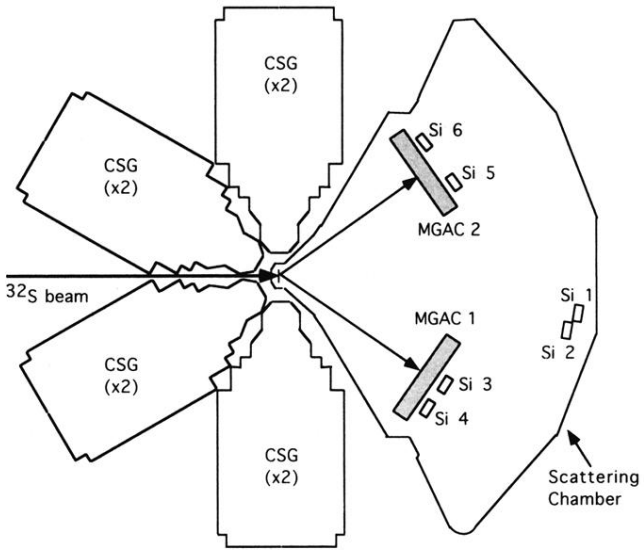

FIG. 1. Schematic drawing of the experimental arrangement. Note that the BGO array of the Argonne-Notre Dame γ-ray facility is not shown for clarity.